Available online at www.sciencedirect.com
SCIENCE DIRECT
Talanta 69 (2006) 906–913
Talanta
www.elsevier.com/locate/talanta

Frequency-selective absorbance detection: Refractive index and turbidity compensation with dual-wavelength measurement

In-Yong Eom, Purnendu K. Dasgupta *

Department of Chemistry and Biochemistry, Texas Tech University, Lubbock, TX 79409-1061, USA

Received 4 October 2005; received in revised form 12 November 2005; accepted 13 November 2005
Available online 20 December 2005

Abstract

A frequency-selective absorbance detection approach and its applications are described. First, a digital signal processor–lock-in amplifier (DSP–LIA)-based absorbance detector was evaluated. Compared to a simple operational amplifier (TL082CP)-based detector, the DSP–LIA-based detector showed lower noise levels, but the relative advantage was reduced under very low photocurrent levels (down to few nA). A 7 cm pathlength flow cell with this commercial LIA-based detector exhibited excellent Beer's law linearity ($r^2 = 0.9999$) and a noise level of 7 micro absorbance units (μAU). The limit of detection (LOD, S/$N = 3$) for methyl orange (MO) was 7 nM with this detector. Finally, as a more affordable alternative to an LIA, a balanced demodulator integrated circuit chip was used to fabricate a dual wavelength–frequency-selective LED-based absorbance detector. This device successfully compensated refractive index (RI) effect and turbidity effect in test flow systems. The LOD for MO with this system was 8 nM.

Keywords: Frequency-selective detection; Dual-wavelength photometry; Refractive index effect; Turbidity effect; Balanced demodulator; Light emitting diode

1. Introduction

Absorption photometry is the most widely used measurement method in analysis in general and in flow-injection analysis (FIA) in particular. FIA has proven to be a suitable technique for a variety of rapid and reproducible analysis needs with rather simple and inexpensive apparatus. The sensitivity and ultimate applicability of optical absorbance detection in FIA is often limited by the refractive index (RI) difference between a sample and the carrier into which the sample is injected. As a result of laminar flow, a continuous concentration gradient is established along the sample zone. The boundary (concave or convex, depending on the direction of view) of the injected fluid (which has a different RI) acts as a lens that either focuses more light on to the photodetector at the other end of the cell or refracts light away on to the wall, resulting respectively in a negative or positive absorbance excursion from the baseline and thus constituting an artifact signal that does not arise from light absorption. Various factors such as the RI difference between the sample and the carrier, the degree of sample dispersion, the cell design, etc. can all affect the magnitude of this effect.

Dual-wavelength spectrophotometry has been successfully used to compensate RI effects in FIA. Zagatto et al. [1] showed the feasibility of this technique. While light passed through the flow cell and after dispersion by a monochromator, the intensities at two selected wavelengths were monitored with a diode array detector. The RI effect compensation was done by real-time subtraction of the wavelength-independent signal (caused by the RI difference) from the signal at the analytical wavelength. Renn and Synovec [2] eliminated the effect of thermally induced RI aberrations by using a fiber-optic-interfaced flow cell and a position sensitive detector. Liu and Dasgupta [3] simultaneously compensated for both RI and turbidity effects using an LED-based, dual-wavelength, double-beam, dual-flow-cell photometric detection system. Other efforts [4–7] have been made to compensate for artifact absorbance signals from RI effects by better cell design.

As the push for detecting smaller and smaller concentrations continues, the need for further improving the sensitivity for absorbance-based detection is also increasing. According to Lambert–Beer's law, the sensitivity of optical absorbance detection can be improved by simply increasing the optical path

* Corresponding author.
E-mail address: sandy.dasgupta@ttu.edu (P.K. Dasgupta).

0039-9140/$ – see front matter © 2005 Elsevier B.V. All rights reserved.
doi:10.1016/j.talanta.2005.11.033

length without changing any other factor. Since the report of the first light emitting diode (LED)-based absorbance detector that utilized a 30-cm path length [8], LEDs have been used to develop long path optical detection systems [9–11]. However, normally the noise level increases as the path length increases because light diverged to the cell walls is lost. It is widely believed that the pathlengths that are too long cause the detector to be light-starved and deteriorate the S/*N*. One rarely encounters standard flow cells with a path length greater than 20 mm in FIA.

A simple, useful approach that has become very widely used recently is to minimize source light loss to the cell by the use of a liquid core waveguide (LCW) cell. In an LCW cell, the tube material (cladding) has a lower RI than that of the fluid (core). The source light thus propagates through the LCW fluid by total internal reflection (TIR). An amorphous fluoropolymer, Teflon® AF (RI ~ 1.29–1.31, water RI in 1.33) is typically used for the construction of LCW cells. Such cells have now been widely used for long path length spectrophotometry [10–22]. However, at a price several times that of gold per unit weight, Teflon® AF is one of the most expensive commercial polymers. Further, Teflon® AF is highly gas permeable and this can cause problems from gas transport through the cell wall, notably external CO_2 can come into the internal solution as well as enhanced evaporation of water from the internal solution can occur. Teflon® AF clad optical quality silica tubes can solve this problem but are available only in very small internal diameters (<100 μm). Moreover, the manufacturer of Teflon® AF now requires all prospective users to sign onerous agreements even before it can be purchased.

An alternative approach is to improve the detectability of low levels of light. If the light is modulated at a fixed frequency, a frequency-selective detector such as a lock-in amplifier (LIA) can be used to remove unwanted noise from a signal; such devices provide a DC output corresponding to the amplitude of the signal at the chosen frequency. The cost of high performance LIAs has decreased dramatically in recent years thanks to the availability of high-speed digital signal processor (DSP) chips. The lock-in detection technique is both frequency-sensitive and phase-sensitive although in absorbance detection systems, the latter aspect is generally not used. Frequency-sensitive detection can extract individual signals from two light sources modulated at different, anharmonic frequencies, registered by the same detector. Aside from stand-alone LIA units, commercially available cost effective LIA modules that can be put as a card inside a PC are also available [23,24]. National Instruments provides software-based LIA modules for their widely used LABVIEW™ program [25]. Many applications of computer-interfaced LIAs based on commercially available modular, digital processor boards have been reported [26–28].

Fast on/off speed, high repeatability, and negligible warm-up time make LED light sources ideally compatible with a LIA-based photometric detection. Hauser and his students have carried out early pioneering work in this area. Hauser and Liang [29] reduced noise induced by ambient light by using an LIA for membrane-based gas detector in which the sensor tip was exposed to ambient light. The system was used for sensing of ammonia and carbon dioxide in the vapor phase. Hauser and Tan [30] also used a balanced demodulator integrated circuit (IC), a poor man's LIA as it were, to determine oxygen and nitrate with a membrane-based fluorescence sensor. The balanced demodulator circuitry cannot directly provide phase selectivity but can provide frequency-selective detection. A bifurcated fiber optic combined with a sensing membrane was used with an LED as an excitation source and a photodiode as a detector. The balanced demodulator circuitry was adopted to discriminate the analytical signal from that caused by ambient light. Suzuki et al. [31] have described a multiple-LED multichannel LIA-based absorbance detector for the determination of iron in river samples with a FIA system.

Here, we compare the performance of a DSP-based LIA as a single wavelength LED-source absorbance detector with a modest path length (7 cm) cell with that of a simpler more conventional single-chip operational amplifier-based absorbance detector. We also report on the ability of a two-wavelength detector based on two balanced demodulators to provide individual frequency-selective detection and apply this to both the compensation of refractive index effect and the determination of the colorant in a turbid sample.

2. Experimental

2.1. Flow-injection systems and reagents

The evaluation of the commercial DSP-based LIA (SR830, Stanford Research Systems, Sunnyvale, CA)-based absorbance detector was carried out with a rudimentary single line flow-injection system with a manually operated six-port injector (7000 series, Rheodyne) equipped with a ~100 μl loop. To minimize dispersion effects, the injector and the detector were connected with a minimum length of tubing with an estimated volume of 30 μl. NaOH solution (1 mM) was used as both the carrier solution and the sample medium. Gravimetric flow (~0.2 ml/min) was used to eliminate noise arising from pulsation and hence to find ultimately attainable LODs.

The flow system for the dual-wavelength LED-based photometric detection system with balanced demodulators is schematically depicted in Fig. 1. A more realistic dual-line manifold was used [1]; this also avoids the high degree of noise caused simply by injector actuation in a single line system. A mixing coil (~25 cm out of 40 cm length of 0.71 mm i.d. Teflon tubing was knotted, knot diameter ~3 mm) was added to allow better mixing. A peristaltic pump (Dynamax, Rainin) propelled the sample carrier (0.74 ml/min) stream in which the injector was located.

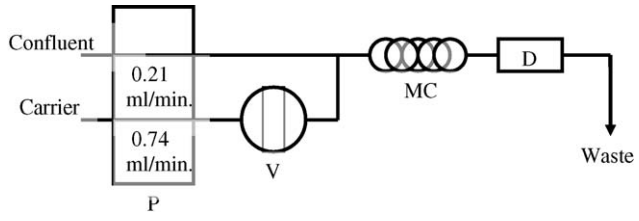

Fig. 1. Schematic representation of the two line flow system for RI compensation experiment: P, pump; V, six-port valve; MC, mixing coil; D, detector.

The confluent stream was pumped peristaltically at 0.21 ml/min. The injection volume was ~135 μl.

Methyl orange (MO, J.T. Baker), cresol red (CR, Aldrich), and other chemicals were used without further purification. A stock MO solution (0.5 mM) was prepared and diluted as needed. Deionized water was used both as the carrier and confluent fluid for the dual-wavelength RI compensation experiment. To induce RI effects, reagent grade NaCl (1–4%, w/v, Mallinckrodt) was added to the MO working solutions. As a point of reference, the high end of this range approximately corresponds to the total salt content of sea water. Cresol red and homogenized milk (Milk Chug™, Dean Foods Co., Albuquerque, NM) were used respectively as the colorant and the turbidity-inducing component. A stock solution of CR (1 mM) was used to prepare a series of calibration solutions and stock milk (1%, v/v) solution was used to prepare samples of different levels of turbidity but containing the same level of the colorant. As the matrix and for all dilution steps, 1 mM NaOH solution was used. This was also used as the carrier solution for this turbidity compensation experiment.

2.2. *z-Path flow-through cells and optoelectronic components*

2.2.1. *Commercial LIA-based absorbance detector*

A homemade 7 cm pathlength z-path flow-through cell, as shown in Fig. 2, was used in these experiments. A Teflon tubing (0.86 mm i.d., 1.57 mm o.d.) was forcibly inserted into a bigger Teflon tubing (1.50 mm i.d., 2.31 mm o.d.) and then this nested tube system was inserted into a stainless steel tube (9 cm long, 2.39 mm i.d., 3.05 mm o.d.) which had holes drilled in it, 1 cm apart from each end of the tube. Two 20 gauge stainless steel tubes were cemented through these holes at ~45° from the cell body. Optical fibers (1 mm core diameter) were inserted and fit tightly into the inner Teflon tube ends to complete the z-path cell and to launch/receive LED source lights. The estimated cell volume was 41 μl.

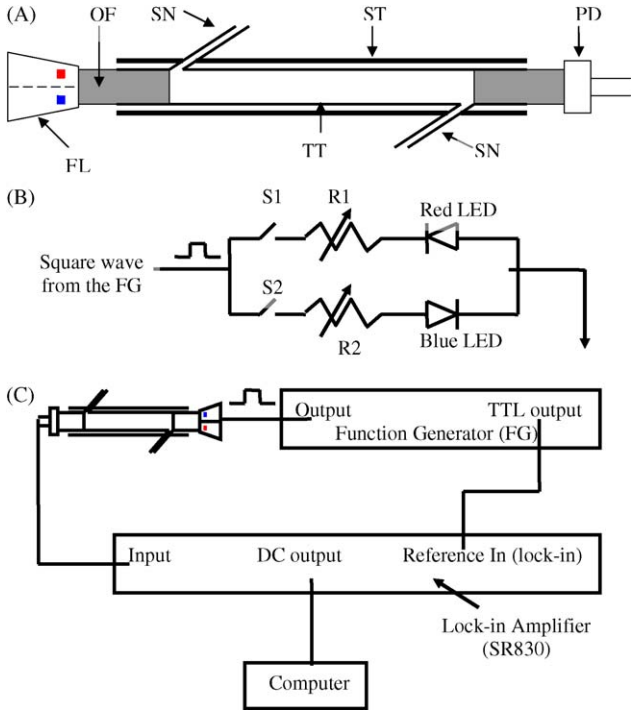

Fig. 2. Schematic representation of the fabricated z-path flow-through cell and detection system: (A) z-path flow-through cell, (B) fused LED modulating format; each LED could be turned off by switches S1, S2, and (C) block diagram of the fused two-color LED modulation and detection with a LIA: OF, optical fiber; ST, stainless steel tube jacket; PD, photodiode; TT, Teflon tubes; SN, stainless steel needle; FL, fused two-color LED; black squared dots in the FL represent the LED chips.

A small silicon photodiode (3 mm × 3 mm active area, BPW34, Siemens) was cemented on the end of the receiving optical fiber and wrapped by aluminum foil, which was grounded to provide shielding and immunity from ambient light. A two-color "fused" LED was fabricated with a red LED (λ_{peak} = 621 nm, Stanley) and a blue LED (λ_{peak} = 468 nm, Nichia). The side walls of each LED were removed, polished, and then they were cemented together. The dome part of the cemented LED was also removed down to a height of ~0.5 mm from the emitter chips and then polished again. The free end of the light input fiber optic was glued to the emitter end of the fused two-color LED and the whole covered with carbon-doped black epoxy. Electrically, the two LEDs were connected in parallel but with a reversed polarity.

The function generator (Model 3011, Dynascan Corp.) modulated the two-color LED at 200 Hz (square wave). Variable resistors (0–500 Ω) were used to limit the current for each emitter (Fig. 2B). The PD output was directly fed to the LIA current input port and the DC output from the LIA was collected by a laptop computer through a 16-bit interface A/D–D/A board (PCM-DAS16/16AO, Measurement Computing Corp., Middleboro, MA). The LIA output is essentially the difference in the transmittance signal between the two wavelengths. In our experiments, the blue LED provided the analytical wavelength of interest and the red LED provided a reference wavelength. The individual LED output intensities can be varied by adjusting R1 and R2 (Fig. 2B). Thus, by equalizing the photocurrents at each wavelength registered on the photodiode by the adjustment of R1 and R2, the LIA output can be set to zero (or to any other desired value) for the detector baseline. For experiments where detector performance at a single wavelength was ultimately of interest, we had expected that using the second LED as a reference will still have some benefits, e.g., it may compensate for flow noise. At least for experiments conducted with gravity flow where flow noise was practically nonexistent, no significant improvement in noise performance was observed between pulsing only the blue LED relative to alternately pulsing the two LEDs in the fashion described. These results are therefore reported without distinction.

The TTL output of the function generator (200 Hz) was fed to the reference input of the LIA. The LIA output corresponded to ~0° phase shift such that the LIA output decreased as the intensity of the transmitted blue light decreased. The detector output was taken to correspond to 100% T with all drive currents adjusted as desired and the carrier fluid flowing through the cell. Then, the blue LED was turned off to determine 0% T. Software written for the purpose and resident on

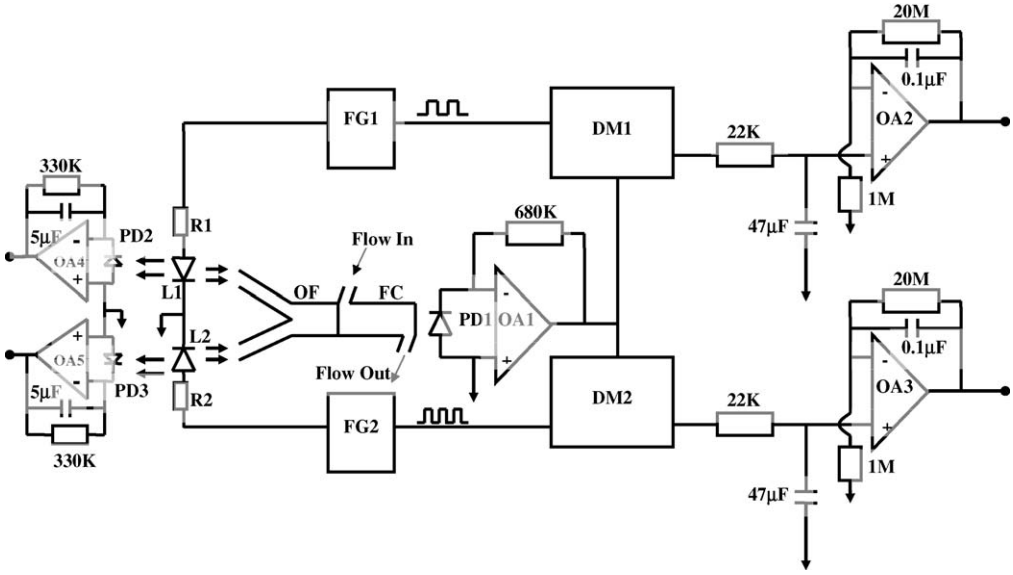

Fig. 3. Schematic representation of the dual-wavelength LED-based photometric detection system with balanced demodulators: two LEDs are fully referenced. L1: analytical wavelength LED; L2: reference wavelength LED; R1 and R2: current limiting variable resistance; OF: bifurcated optical fiber; FC: fiber optic-based demountable z-path flow-through cell; FG1 and FG2: function generators; PD: photodiodes; DM1 and DM2: balanced demodulators (AD630AD); OA: op-amp (TL082CP).

the data acquisition PC converted the measured transmittance signal into absorbance values. The LIA time constant was set to 1 s.

2.2.2. *Single wavelength operational amplifier or commercial current amplifier-based absorbance detector*

A simple single wavelength operational amplifier-based absorbance detector was taken as the benchmark for comparison. The photocurrent of the detector photodiode was converted to voltage by a conventional current → voltage conversion arrangement using a gain of 4×10^7 V/A. A feedback resistor of 40 MΩ with a 50 pF capacitor in parallel provided a time constant of 2 s. The light source was a 468 nm blue LED (Nichia, identical to that used in the two-color LED) driven by 20 mA dc. Both for the LIA and the operational amplifier-based detector, all data were collected at 10 kHz and averaged on the fly with a 1-s average.

2.2.3. *Dual-wavelength LED-based photometric detection system with balanced demodulators—refractive index or turbidity compensation*

This experiment utilized a 1 cm path length fiber optic coupled flow-through cell. A previously described design [32] was used without the focusing lens. This flow-through cell is composed of two aluminum blocks (one block holds a bifurcated fiber optic and the other block holds a photodiode) sandwiching a translucent Kel-F® block which contains a z-path flow passage (1.5 mm i.d. and 10 mm length) with a cell volume of ∼18 μl. The translucent body normally needs an opaque covering to prevent the intrusion of ambient light in absorbance measurements. However, with frequency-selective detection providing immunity against ambient light fluctuations, no efforts were made to shield the cell from ambient light. Balanced demodulator IC's (AD630AD, Analog Devices Inc.) were used with low-pass filters in these experiments to achieve frequency-selective synchronous detection. The electronic circuitry suggested by the manufacturer [33] was used without modification.

The complete electronic circuitry of the dual-wavelength LED-based photometric detection system with balanced demodulators is schematically shown in Fig. 3. A blue LED (λ_{peak} = 468 nm, Nichia) was used as the analytical wavelength for the detection of MO dye only and a red LED (λ_{peak} = 660 nm, Kingbright) was chosen as the reference wavelength for the refractive index (RI) compensation. Two function generators (FG5010, Tektronics) operated both LEDs independently at different frequencies with square wave excitation (700 Hz for the blue LED, 1.0 kHz for the red LED). The bifurcated fiber optic conducted the two-color LED source light to the cell. The light passed through the flow cell and registered on the photodiode (PD). The photocurrent was first amplified by OA1 with a gain of 6.8×10^5 V/A, and then fed in parallel to two demodulators DM1 and DM2 (AD630AD). Each of the modulator outputs contained only the corresponding LED transmittance signals—these were filtered with low-pass filters (22 KΩ and 47 μF) and amplified, the final stage with a time constant of 2 s. These signals were stored by the laptop computer with 16-bit resolution. The LED light sources were fully referenced by cementing individual photodiodes PD2 and PD3 at the bottom of the LEDs [32] to collect back-scattered light. These reference signals were amplified by OA4 and OA5 with a gain of 3.3×10^5 V/A, and filtered through low-pass filters (RC = 1.7 s). The negative log of the quotient of the demodulator signal to the corresponding reference diode signal was computed by the PC as the absorbance value.

Turbidity compensation was accomplished through the same flow manifold and detection system. Cresol red (CR) was used as a colorant and whole milk was used to cause turbidity. For this experiment, a green LED (567 nm, Stanley) was used as the analytical wavelength source and an IR LED (940 nm, LEDtronics) was used as a reference wavelength source. A

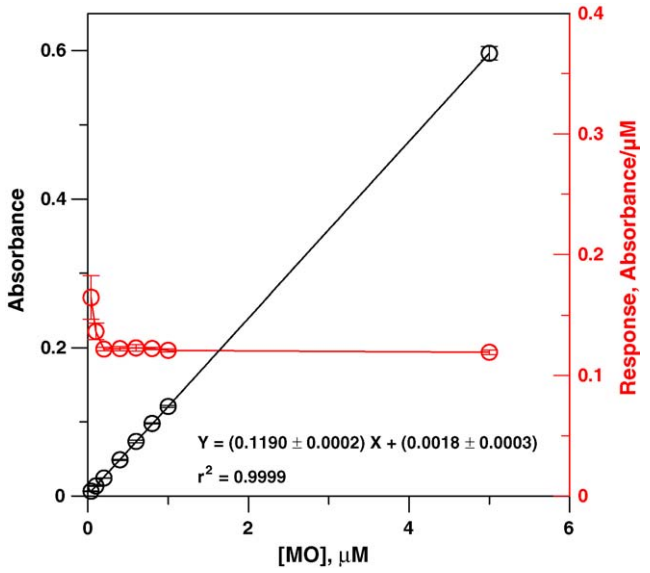

Fig. 4. Circles: calibration curve of methyl orange (MO) for the 7 cm path length cell with the DSP–LIA absorbance detector and diamonds (right ordinate): a response uniformity plot, often called a Cassidy plot.

0.7 KHz square wave was used to operate a green LED and 1 KHz was used for a reference IR LED. Pure cresol red (CR) solutions were used for calibration and then a series of cresol red solutions made varyingly turbid by adding whole milk were prepared and then injected. 1 mM NaOH was used for both a sample medium and a carrier solution.

3. Results and discussion

3.1. Performance comparison between the DSP–LIA-based detector and a simple operational amplifier-based detector

Fig. 4 shows the excellent Beer's law linearity observed for the concentration–absorbance plot for MO over the 40 nM–5 μM range determined for the 7 cm path length cell. A response uniformity plot (Cassidy plot [34]) is also shown. The linear correlation coefficient was 0.9999 with a *y*-intercept statistically indistinguishable from zero. At a LED drive current of 20 mA (reference LED drive current 10 mA), the noise level of the LIA-based detector was 7×10^{-6} absorbance units (AU), corresponding to an S/*N* = 3 LOD of ~6 nM. Noting that this is a 7 cm cell, in terms of S/*N* that will correspond to the performance of conventional 1 cm cell, the noise level is equivalent to 1 μAU. This compares favorably with the performance of the best commercially available detectors today. Under the same conditions, the benchmark consisting of the simple operational amplifier-based detector had a noise of 300 μAU, some 40 times worse.

3.2. Noise levels as a function of detector photocurrent

For our 7 cm path length cell, the 7 μAU noise of LIA-based detector reached with a LED drive current of 20 mA (detector photocurrent ~150 nA) did not markedly decrease at higher LED drive currents. As the detector photocurrent was reduced deliberately to 73, 25 and 13 nA by reducing the LED drive current, the noise increased to ~14, ~16 and ~100 μAU. Remarkably, while the noise on the op-amp-based detector increased, it did so at a less precipitous rate, especially at very low photocurrents; the corresponding values were ~1.5, 3–3.5 and 3–3.5 mAU at the three LED drive current levels (note that the time constant on this detector was twice that of the LIA-based detector).

Other experiments were conducted to confirm that the noise is primarily a function of the detector photocurrent. With a photodiode detector and an LED source and the present LIA, we observed that as long as the current level measured by the LIA was approximately the same, the specific geometries (LED and PD at ends of an air-filled 7 cm long PTFE tube, LED and PD coupled by short 2 mm optical fiber lengths, LED and PD coupled head to head) did not affect the ultimately observed short-term (2 min) noise level, which remained in the range of 7–20 μAU.

We also experimented with an LED–LED pair. Light emitting diodes are bidirectional transducers although they are much poorer detectors than emitters. Nevertheless, driving a blue LED as an emitter at ~20 mA while using a second blue LED as the detector resulted in a respectable short-term noise level of 35 μAU. While this was not pursued in the present work, continuous alternation of source-detector identities (at a rate that is fast compared to the passage of a fluid element through the cell) can in principle compensate for refractive index induced optical effects.

Finally, the dependence of the detector noise on the detector photocurrent was measured over a large range of detector photocurrent (6–10 000 nA) by using a directly (head–head) coupled LED–PD arrangement. As a readily available i → V converter, a commercial current amplifier (Keithley 427) was used, with a 300 ms time constant. The best description of the noise as a function of photocurrent was a linear decrease in noise with the logarithm of the photocurrent:

$$\text{Noise, AU} = Y = -7.07\text{e}-4\log(\text{photocurrent, nA}) + 3.12\text{e}-3, \qquad r^2 = 0.9320 \tag{1}$$

With the LIA and operational amplifier-based arrangements, similar equations where:

$$\text{Noise}\,(N) = a\log(i_{\text{detector}}) + b \tag{2}$$

were also found to describe the observed behavior.

3.3. Is there an optimum cell path length based on noise?

If the system noise is ultimately governed by light intensity reaching the detector, it may be possible to determine the best cell path length for any given measurement approach. In any given flow cell of significant length, Beer's law behavior requires that the light transmitted decreases exponentially with the length due to wall losses, regardless of attenuation by the fluid in the cell:

$$I_L = I_0 \times 10^{-\alpha L} \tag{3}$$

where I_L is the intensity of the light after traversing length L, α the attenuation coefficient, and I_0 is the initial light intensity. For a 1.68 mm i.d. glass tube 350 μm in wall thickness, externally silvered and probed with 466 nm light, the fit to Eq. (3) is very good (linear $r^2 = 0.9926$) for L up to 20 cm with the best fit α value of 0.0617/cm. In optical fiber terms, this corresponds to an attenuation factor of 62 dB/m. In comparison, the data of Toda et al. [35] for a 1.1 mm i.d. Teflon® AF tube corresponded to an attenuation factor of just over 35 dB/m.

Practical cell path lengths will most often be dictated by maximum desired cell volume, pressure drop, dispersion, characteristics, etc. Nevertheless, aside from such considerations, it is of interest if there is some optimum cell length from an S/*N* point of view. It may appear at first sight that there is some optimum path length beyond which the increased signal (linearly related to the path length L, as long as Beer's law is obeyed) will be more than offset by the increased noise, i.e., there may be a maximum in L/N (tantamount to S/*N*), or conversely, a minimum in N/L. Surprisingly, as long as the behavior is dictated by Eqs. (2) and (3), no such maxima/minima are to be expected. Considering that i_{detector} of Eq. (2) must be linearly related to I_L of Eq. (3), we can divide Eq. (2) by L and write:

$$\frac{N}{L} = \frac{a\log(k \times 10^{-\alpha L}) + b}{L} = \frac{a\log k + b}{L} - a\alpha \tag{4}$$

It is obvious that N/L will continue to decrease with increasing L and does not have a minimum and no magic optimum therefore exists. The race for very long path absorbance measurement cells, already many meters in length [15,36,37], can therefore justifiably continue.

3.4. Refractive index (RI) compensation with a two-channel balanced demodulator detector

A balanced demodulator can provide frequency-selective detection albeit not phase-selective detection, unlike an LIA. This is nevertheless perfectly acceptable for absorbance detection. Before actually testing the applicability in RI compensation, two red LEDs (660 nm), a photodiode, and a bifurcated fiber optic were used to check if two modulators could adequately discriminate between two signals at anharmonic frequencies without cross-talk. This experiment showed that changing the drive current of an LED changed the dc output level of the corresponding demodulator while the detector output corresponding to the other LED was not affected. In other words, no cross-talk between the two demodulators was observed. The actual experiment was then conducted with a 468 nm (analytical wavelength where MO absorbs) LED and a 660 nm LED driven respectively at 20 and 7 mA (this compensates for the higher emitter and detector efficiency in the red).

Unlike previous experiments with gravimetric flow, these experiments were conducted with a peristaltic pump and resulted in substantial flow noise. The observed noise (without any baseline correction) was 190 and 140 μAbs at 468 and 660 nm, respectively. Simply subtracting the 660 nm absorbance from the 468 nm absorbance reduced the flow noise to 80 μAbs.

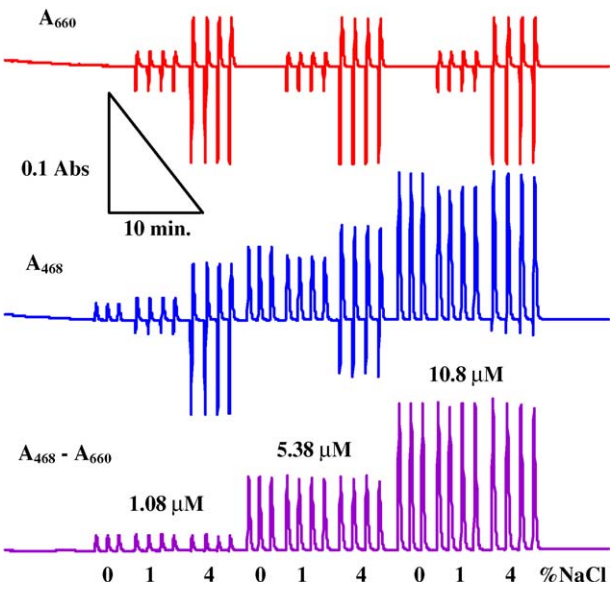

Fig. 5. Results of refractive index (RI) compensation arrangement of methyl orange (MO); NaCl content varies 0–4% (w/v) and MO varies 1.08–10.8 μM. A_{468}, absorbance at analytical wavelength; A_{660}, absorbance at reference wavelength; A_{468}–A_{660}, corrected absorbance by real-time subtraction method (each subscript refers to peak wavelength of source LED). The abscissae markings indicate the %NaCl concentration in the sample for each group of triplicate/quadruplicate injections.

In the present system, injection of a pure NaCl solution into a water carrier will result in a bidirectional signal with the absorbance first going negative and then going positive. Fig. 5 shows three rows of traces, from the top: the apparent absorbance at 660 nm, that at 468 nm, and the difference between the two. Each row contains the results of nine sets of injections ($n = 3$ or 4 each), 1.08, 5.38 and 10.8 μM MO containing 0, 1, and 4% NaCl. Note that 660 nm results are tantamount to having only NaCl injected as MO has no absorption at 660 nm. The negative going initial RI induced response is not always observed in the 468 nm trace; especially at higher MO and lower NaCl concentrations because the effects are additive and the absorption by MO obscures the RI effect, which nevertheless underlies the observed response.

In most cases, RI and absorption effects can be assumed to be strictly additive and adequate compensation can be obtained [1]. This appears to be the case in the present system; the maximum error after correction is 3% whereas before correction it ranges up to 256% (Table 1). Corrections can also be done based on peak area additivity and has been recommended in the presence of significant pump noise [3]. However, this did not appear necessary in the present case.

3.5. Turbid samples—how much colorant in milk?

To illustrate the feasibility of applying frequency-selective dual-wavelength photometry to turbid samples, we determined the content of a colorant in homogenized milk using the same FIA and detection system as above. As a simulant for chocolate syrup or strawberry syrup, we used the dye cresol red (CR). Responses of pure CR standards at analytical wavelength, over

Table 1
Methyl orange absorbance signals with and without the presence of NaCl with and without dual-wavelength correction (% errors are in parenthesis)

[MO] (μM)	NaCl, % (w/v)	Absorbance (peak height) (Abs)	
		Before correction A_{468} only (% error)	After correction A_{468}–A_{660} (% error)
1.08	0	0.0131	0.0132
1.08	1	0.0169 (29)	0.0134 (1.5)
1.08	4	0.0466 (256)	0.0128 (−3.0)
5.38	0	0.0609	0.0608
5.38	1	0.0518 (−15)	0.0602 (−1.0)
5.38	4	0.0773 (27)	0.0597 (−1.8)
10.8	0	0.1222	0.1220
10.8	1	0.1099 (10)	0.1216 (−0.3)
10.8	4	0.1209 (1)	0.1219 (−0.1)

a 2.12–10.16 μM concentration range, were highly linear:

$$A_{567}(\mathrm{CR}) = (0.02344 \pm 0.00013)[\mathrm{CR}] + (0.00352 \pm 0.00093), \qquad r^2 = 0.9999 \tag{5}$$

Turbid samples with different concentrations of CR were prepared (Fig. 6). A simple linear subtraction method was applied to predict the cresol red (CR) content in milk.

$$A_{567} = A_{567}(\mathrm{M}) + A_{567}(\mathrm{CR}) \tag{6}$$

$$A_{940} = A_{940}(\mathrm{M}) + A_{940}(\mathrm{CR}) \tag{7}$$

where A_{567} and A_{940} are absorbance signals from turbid CR samples at analytical and reference wavelengths and (M) and (CR) imply absorbance signals caused by absorption of milk and CR, respectively. CR has no significant absorption at 940 nm (A_{940} (CR) = 0). A turbidity ratio at the two wavelengths, K_T can

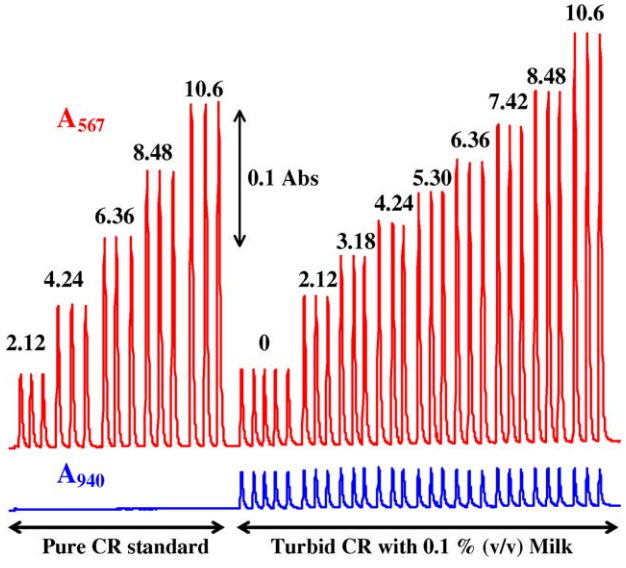

Fig. 6. Absorbance outputs from analytical (A_{567}) and reference (A_{940}) wavelengths for pure CR standard and turbid CR samples (each subscript refers to peak wavelength of source LED). Concentration of CR for each sample is shown on the corresponding peaks in μM.

Table 2
Results of a determination of cresol red content in milk with dual-wavelength photometry

$[\mathrm{CR}]_{\mathrm{Taken}}$ (μM)	$[\mathrm{CR}]_{\mathrm{Predicted}}$ (μM)	% Error
2.12	2.08	−1.7
3.18	3.16	−0.5
4.24	4.24	0.0
5.30	5.21	−1.7
6.36	6.31	−0.8
7.42	7.36	−0.8
8.48	8.35	−1.5
10.6	10.2	−3.7

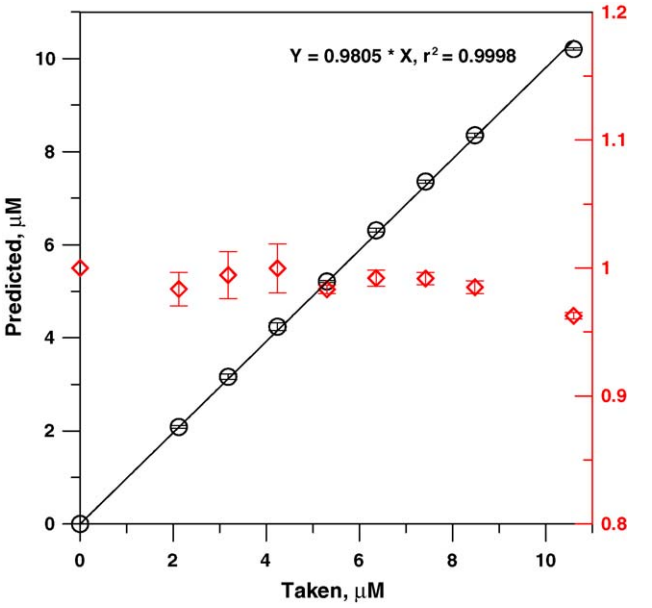

Fig. 7. Cresol red content in milk; circles: actual concentration taken vs. that computed from the results. Diamonds (right ordinate): Cassidy plot: computed to actual concentration quotient vs. actual concentration.

be defined as:

$$K_T = \frac{A_{567}(\mathrm{M})}{A_{940}(\mathrm{M})} \tag{8}$$

For the present system, K_T was found to be a constant. Based on injections of 0.1% milk, K_T was determined to be 2.12 ± 0.06. Rearranging Eqs. (6)–(8), the true absorption due to CR can now be calculated from Eq. (9):

$$A_{567}(\mathrm{CR}) = A_{567} - K_T A_{940} \tag{9}$$

and the true CR content of the milk samples can be obtained from Eq. (5). Table 2 and Fig. 7 show that excellent recovery of CR can be obtained. Turbidity correction was done based on peak height additivity was done in the off-line mode but on-line and real-time subtraction method can be applied if the baselines for both signals (A_{567} and A_{940}) are adjusted to zero.

4. Conclusions

The performance of a high quality LIA-based absorbance detector was compared with a simple op-amp (TL082CP)-based

absorbance detector. With adequate source intensity, the LIA-based absorbance detector showed substantially lower noise levels than those of the TL082CP-based absorbance detector. However, when both detectors were tested with very low source light intensity (down to few nA photocurrent), the relative advantage was reduced, although the LIA continued to perform better. This was not anticipated. We had expected a dual-wavelength LIA to be relatively immune to flow noise. This was not the case, either. Nevertheless, under optimum conditions, very low absolute noise levels could be obtained with an LIA-based absorbance detector. With methyl orange (MO) solutions, a good linearity ($r^2 = 0.9999$) for over 2 orders of magnitude concentration range (40 nM–5 μM) was achieved with a 7 cm length z-path flow-through cell. A 7 nM LOD ($S/N = 3$) of MO could be achieved.

A balanced demodulator chip provides a more affordable alternative to an LIA. A dual wavelength–frequency-selective LED-based photometric detection system based on balanced demodulators was fabricated and tested for RI compensation with a fiber optic-based demountable z-path flow-through cell. This provides a relatively simple and affordable approach to general photometric analysis. Refractive index effects were compensated successfully by subtracting the absorbance at a reference wavelength from that at the analytical wavelength. Further, we were able to demonstrate the compensation for a turbidity causing while measuring the concentration of a dye added to a turbid sample.

Frequency-selective detection has many merits. These include immunity to ambient light fluctuations, ability to work at lower photocurrents, and the ability to work at multiple wavelengths with a single detector as long as the sources can be separately modulated. The latter aspect can be particularly valuable in a variety of situations.

Acknowledgments

This work was supported by Paul Whitfield Horn Professorship funds at Texas Tech University and the detector development was supported in part by the US Environmental Protection Agency through STAR grant RD 83107401-0. However, this manuscript has not been reviewed by the Agency and no endorsement should be inferred.

References

[1] E.A.G. Zagatto, M.A.Z. Arruda, A.O. Jacintho, I.L. Mattos, Anal. Chim. Acta 234 (1990) 153–160.
[2] C.N. Renn, R.E. Synovec, Anal. Chem. 63 (1991) 568–573.
[3] H. Liu, P.K. Dasgupta, Anal. Chim. Acta 289 (1994) 347–353.
[4] J.E. Stewart, Appl. Opt. 20 (1981) 654–659.
[5] J.E. Stewart, Proc. SPIE 492 (1984) 529–534.
[6] H.S. Bellamy, H. Liu, P.K. Dasgupta, Talanta 40 (1993) 341–345.
[7] P.S. Ellis, A.J. Lyddy-Meaney, P.J. Worsfold, I.D. McKelvie, Anal. Chim. Acta 499 (2003) 81–89.
[8] H. Flaschka, C. McKeithan, R.M. Barnes, Anal. Lett. 6 (1973) 585–594.
[9] S. Karthikeyan, S. Hashigaya, T. Kajiya, S. Hirata, Anal. Bioanal. Chem. 378 (2004) 1842–1846.
[10] S.Q. Tao, C.B. Winstead, H. Xian, K. Soni, J. Environ. Monitor. 4 (2002) 815–818.
[11] Q.Y. Li, K.J. Morris, P.K. Dasgupta, I.M. Raimundo, H. Temkin, Anal. Chim. Acta 479 (2003) 151–165.
[12] T. Dallas, P.K. Dasgupta, Trends Anal. Chem. 23 (2004) 385–392.
[13] S.Q. Tao, S.F. Gong, L. Xu, J.C. Fanguy, Analyst 129 (2004) 342–346.
[14] H. Larsson, P.K. Dasgupta, Anal. Chim. Acta 485 (2003) 155–167.
[15] M.R. Callahan, J.B. Rose, R.H. Byrne, Talanta 58 (2002) 891–898.
[16] W.S. Yao, R.H. Byrne, R.D. Waterbury, Environ. Sci. Tech. 32 (1998) 2646–2649.
[17] R.L. Johnson, J.H. Aldstadt, Analyst 127 (2002) 1305–1311.
[18] J.Z. Zhang, J. Chi, Environ. Sci. Tech. 36 (2002) 1048–1053.
[19] J.Z. Zhang, C. Kelbe, F.J. Millero, Anal. Chim. Acta 438 (2001) 49–57.
[20] W.B. Du, F. Qun, Z.L. Fang, Chem. J. Chin. Univ. 25 (2004) 610–613.
[21] K. Toda, K.I. Yoshioka, S.I. Ohira, J.Z. Li, P.K. Dasgupta, Anal. Chem. 75 (2003) 4050–4056.
[22] M.R. Milani, P.K. Dasgupta, Anal. Chim. Acta 431 (2001) 169–180.
[23] http://www.femto.de/index.html.
[24] http://www.dlinstruments.com/products/index.html.
[25] http://digital.ni.com/express.nsf/bycode/lockin?opendocuments&lang=&node=.
[26] J. Berger, D.S. Tannhauser, Rev. Sci. Instrum. 54 (1983) 1781–1783.
[27] L.A. Barragan, J.I. Artigas, R. Alonso, F. Villuendas, Rev. Sci. Instrum. 72 (2001) 247–251.
[28] R. Alonso, F. Villuendas, J. Borja, L.A. Barragan, I. Salinas, Meas. Sci. Tech. 14 (2003) 551–557.
[29] P.C. Hauser, C.L.C. Liang, Instrum. Sci. Tech. 25 (1997) 147–156.
[30] P.C. Hauser, S.S.S. Tan, Analyst 118 (1993) 991–995.
[31] Y. Suzuki, H. Hori, M. Iwatsuki, T. Yamane, Anal. Sci. 19 (2003) 1025–1028.
[32] P.K. Dasgupta, H.S. Bellamy, H. Liu, J.L. Lopez, E.L. Loree, K.J. Morris, K. Petersen, K.A. Mir, Talanta 40 (1993) 53–74.
[33] http://www.analong.com/UploadeFiles/Data_Sheets/106127811AD630_e.pdf.
[34] R.M. Cassidy, L.C. Chen, LC-GC Mag. 10 (1992) 692–696.
[35] K. Toda, K.-I. Yoshioka, S.-I. Ohira, J. Li, P.K. Dasgupta, Anal. Chem. 75 (2003) 4050–4056.
[36] W.S. Yao, R.H. Byrne, Talanta 48 (1999) 277–282.
[37] E.T. Steimle, E.A. Kaltenbacher, R.H. Byrne, Mar. Chem. 77 (2002) 255–262.